An Accurate Analytical Model for Tunnel FET Output Characteristics

Yunhe Guan, Zunchao Li, Hamilton Carrillo-Nuñez, Yefei Zhang, Vihar P. Georgiev, *Member*, *IEEE*, Asen Asenov, *Fellow*, *IEEE*, and Feng Liang

***Abstract*—The analytical models for the output characteristics of tunnel FETs (TFETs) based on Maxwell-Boltzmann (MB) statistics have some accuracy issues, especially in linear region of operation, when compared with more sophisticated numerical approaches. In this letter, by exploiting the thermal injection method (TIM), an accurate analytical model for the TFET potential profile is proposed. Although the approach is initially envisaged for heterojunction TFETs (H-TFETs), it could be straightforwardly adopted for homojunction TFETs. After an accurate description of the potential profile is obtained, the current is then computed by means of a Landauer-like expression. Comparison with numerical simulations at different bias conditions shows that the predicted output characteristics qualitatively improve, leading to a significant enhancement in accuracy at a much less computational cost.**

***Index Terms*—Analytical model, Maxwell-Boltzmann statistics, Tunnel FET, Thermal injection method.**

I. Introduction

An analytical potential model considering Fermi-Dirac (FD) statistics is difficult to derive due to the numerical implementation of the FD integral [1]. As a consequence, a variety of models reported in the literature [2]–[5] have to resort to Maxwell-Boltzmann (MB) statistics due to its simplicity, despite some iterations involved. However, MB statistics becomes questionable and it is expected to provide less accurate results when simulating the carrier transport in tunnel FETs (TFETs) [6].

In this letter, a new analytical potential model is developed for double-gate (DG) heterojunction TFETs (H-TFETs) (Fig. 1(a)) by adopting the thermal injection method (TIM), which will be explained in detail later. The problems with inaccuracy and inefficiency associated with the use of MB and FD statistics in the past are successfully evaded.

This work was supported in part by the National Natural Science Foundation of China under Grant 61176038 and Grant 61474093, the Technology Development Program of Shaanxi Province under Grant 2016GY-075, (Corresponding author: Zunchao Li.)

Y. Guan, Z. Li, Y. Zhang, and F. Liang are with School of Microelectronics, Xi'an Jiaotong University, Xi'an 710049, Shaanxi, P. R. China (e-mail: zcli@xjtu.edu.cn).

H. Carrillo-Nuñez, V. P. Georgiev and A. Asenov are with the School of Engineering, University of Glasgow, Glasgow G12 8LT, U.K.

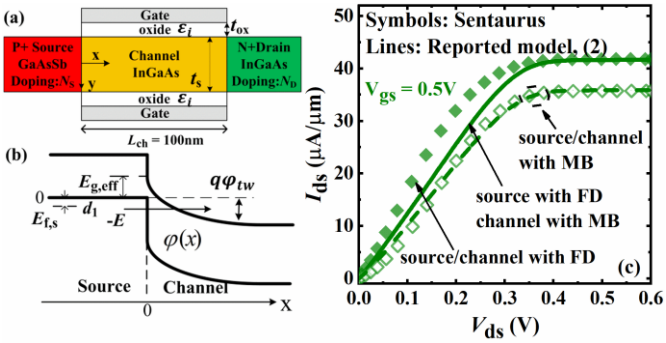

Fig. 1. (a) Structure of DG H-TFET. (b) Sketch of H-TFET band-diagram. (c) I_{ds}–V_{ds} curves from simulations (symbols) and the model given by (2) (lines). The model parameters are: $E_{g,eff}$ = 0.27eV which is in line with [7], d_1 = 0.1eV for $N_v = 8\times10^{18}\text{cm}^{-3}$, $N_c = 2\times10^{17}\text{cm}^{-3}$, $m_e = 0.04m_0$, and $m_h = 0.46m_0$.

II. Theory and Methodology

Fig. 1(a) describes the DG H-TFET considered in this work with the internally lattice-matched $GaAs_{0.5}Sb_{0.5}/In_{0.53}Ga_{0.47}As$ heterostructure, which is popular because it is lattice matched to the InP substrate [7]. The high-k oxide layer HfO_2 is $t_{ox} = 2\text{nm}$ thick. The lightly p-doped channel is with doping of 10^{16}cm^{-3}. The body thickness, source doping, and drain doping are $t_s = 10\text{nm}$, $N_S = 5\times10^{19}\text{cm}^{-3}$, and $N_D = 5\times10^{18}\text{cm}^{-3}$, respectively. Such high doping concentrations have been realized experimentally [8]. The work function of the gate is 4.6 eV which corresponds to TiN metal gate with <200> grain orientation [9] and guarantees that the valence band (VB) at the source aligns with the conduction band (CB) at the channel at $V_{gs} = 0\text{V}$. For the numerical simulations of the test TFET, the commercial TCAD tool Sentaurus-device [10] has been used. The dynamic nonlocal tunneling-path method, FD statistics, and band-gap-narrowing were activated in the simulations. The quantum confinement effects were ignored for sake of simplicity. The parameters for the extraction of the band-to-band tunneling (BTBT) are taken from [7].

A. Analytical Model based on MB statistics

The sketch band-diagram of a H-TFET is shown in Fig. 1(b). $E_{g,eff}$ is the effective tunneling barrier height. For simplicity, the source depletion is ignored and the BTBT is only assumed from source to channel regions. The channel barrier near source can be described by the following exponential profile [1], [3],

$$\varphi(x) = (E_{g,eff} + q\varphi_{tw})\exp\left(-\frac{\pi x}{\lambda}\right) - q\varphi_{tw} \quad (1)$$

$$\varphi_{tw} = \varphi_{tw,MB} = V_{gs} - (4V_t\varepsilon_s\beta\tan\beta)/(t_sC_{ox}), \quad (2)$$

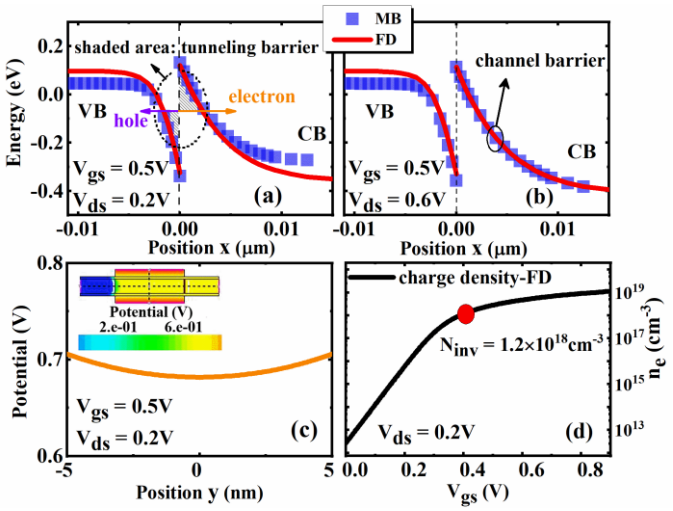

Fig. 2. Band diagrams under FD and MB statistics biased within (a) linear region and (b) saturation region at V_{gs} = 0.5V. The shaded area indicates the tunneling barrier. (c) Potential profile along y axis. Inset is the potential contour. (d) Curve of carrier density vs. V_{gs}. All are obtained from simulations.

where λ is the scaling length [3] and $q\varphi_{tw}$ is the tunneling window. By solving the one-dimensional Poisson's equation, with the carriers obeying a Boltzmann distribution, β is obtained from [3]

$$\frac{V_{gs}-V_{ds}-d_1}{2V_t} - \ln\left(\frac{2}{t_s}\sqrt{\frac{2\varepsilon_s V_t}{qN_c}}\right) = ln\beta - \ln(cos\beta) + \frac{2\varepsilon_s t_{ox}}{\varepsilon_i t_s}\beta tan\beta. \quad (3)$$

V_t is the thermal voltage, N_c is the effective Density-of-States (DOS) of the CB within the channel/drain regions, and $d_1 = kTF_{1/2}^{-1}(0.5N_s\sqrt{\pi}/N_v)$ is the source degeneracy factor, with N_v being the effective DOS of the VB in source region.

For electrons, with effective mass m_e, the current per gate width is given by a Landauer-like equation [4], [11]

$$I_{\rm ds} = \frac{qm_e t_s}{2\pi^2\hbar^3}\int_0^{q\varphi_{tw}} T_{1D}\,(1-e^{-E_t E_{pm}})(f_S - f_D)/(E_t)dE, \quad (4)$$

where $f_{S/D}$ is the occupancy factor at source/drain reservoir. The maximum perpendicular kinetic energy $E_{pm} = \min\{q\varphi_{tw} - E,\ (m_h E)/m_e\}$ assures conservation of perpendicular momentum. 1D tunneling probability T_{1D} and E_t are adopted from [4] without any fitting parameters.

The comparison of $I_{ds} - V_{ds}$ characteristics generated from (4) and numerical simulations is plotted in Fig. 1(c) at $V_{gs} =$ 0.5V. As observed, the saturation is well predicted by both the approaches. However, the former highly underestimates I_{ds} within linear region, which also is apparent at other gate voltages. Such a difference is a direct consequence from employing MB statistics in (2) to calculate φ_{tw}. In order to verify this hypothesis, the simulation result with MB statistics activated is also given by the open symbols in Fig. 1(c). It should be noted that FD/MB statistics can be activated only for the whole device [10]. At this time, the reported model overestimates the current over the entire operation range. This overall mismatch is ascribed to the difference of source degeneracy (i.e. VB) in MB and FD cases, resulting from the high doping, as shown in Fig. 2(a) (linear region) and (b) (saturation region). The difference of channel barrier between MB and FD cases only appears in linear region. Further, by adjusting the lower limit of the integral in (4) to model source degeneracy with MB, the dashed line shows well matched result with the open symbols (Fig. 1(c)).

B. Analytical model based on TIM

From our previous analysis, a good accuracy for predicting the whole $I_{ds} - V_{ds}$ characteristics cannot be guaranteed by (2). Better predictions would be obtained by using FD statistics for the extraction of φ_{tw}. Unfortunately, it is not straightforward to derive an analytical expression for it [1], [2].

Alternatively, considering that inversion charge is injected from drain in TFET, as suggested in Ref. [12], the carrier density in the channel can be described as $n_e = N_D \times e^{-\phi_{CD}(y)/V_t}$, with channel/drain barrier height $\phi_{CD}(y) = d_1 + d_2 + V_{ds} - \varphi_{tw}(y)$. $d_2 = kTF_{1/2}^{-1}(0.5N_D\sqrt{\pi}/N_c)$ is the drain degeneracy factor. The inversion charge per unit area thus can be expressed as

$$Q_e = qN_D\int_0^{t_s} e^{-\phi_{CD}(y)/V_t}\,dy. \quad (5)$$

In ultra-thin body and nanowire TFETs, the variation of the potential profile in a cross section plane is expected to be very weak, as shown in Fig. 2(c) [1]. We therefore assumed φ_{tw} to be constant. Performing calculations of the integral in (5), φ_{tw} can be then computed, by means of Gauss's law and the proper boundary conditions, from

$$qt_s N_D e^{(\varphi_{tw}-d_1-d_2-V_{ds})/V_t} = 2C_{ox}(V_{gs} - \varphi_{tw}). \quad (6)$$

The solution of (6) has a Lambert's W function form. However, an analytical expression for φ_{tw} can be obtained as explained below.

The dependence of carrier density on V_{gs}, obtained from simulation, is shown in Fig. 2(d). Please note that the screening carrier density $N_{\rm inv}$ does not depend on the gate bias. Therefore, it is safe to use the empirical value of $N_{inv} = 1.2\times10^{18}{\rm cm}^{-3}$, based on the following definition, $d\log(n_e)/dV_{gs}|_{N_{inv}} \approx 30\%\max\left(d\log(n_e)/dV_{gs}\right)$. For a Si channel TFET, it is found that $N_{\rm inv} = 1.5\times10^{18}{\rm cm}^{-3}$ is consistent with the empirical value used in Ref. [13]. Although, the slight difference of $N_{\rm inv}$ between the InGaAs and Si channels reveals that $N_{\rm inv}$ weakly depends on the channel material, $N_{\rm inv}$ should be considered as a parameter that is affected by the device parameters, such as body thickness and oxide material, which influence the gate electrostatic control. The stronger the gate control, the higher the screening carrier concentration needed. For instance, $N_{\rm inv} = 2.7\times10^{18}{\rm cm}^{-3}$ when $t_s = 7$nm in case of the InGaAs channel TFET. When $n_e = N_{\rm inv}$, the gate voltage is called the critical voltage V_{cv}, and $\varphi_{tw}(V_{cv}) = d_1 + V_{ds} + d_c$, in which $d_c = kTF_{1/2}^{-1}(0.5N_{inv}\sqrt{\pi}/N_c)$. Before this point, the potential increases almost linearly with V_{gs}, hence we approximate $V_{cv} \approx \varphi_{tw}(V_{cv})$. As a function of V_{gs}, the left-hand-side of (6), namely F, can be approximated by Taylor expansions around $V_{gs} = V_{cv}$ up to the second-order,

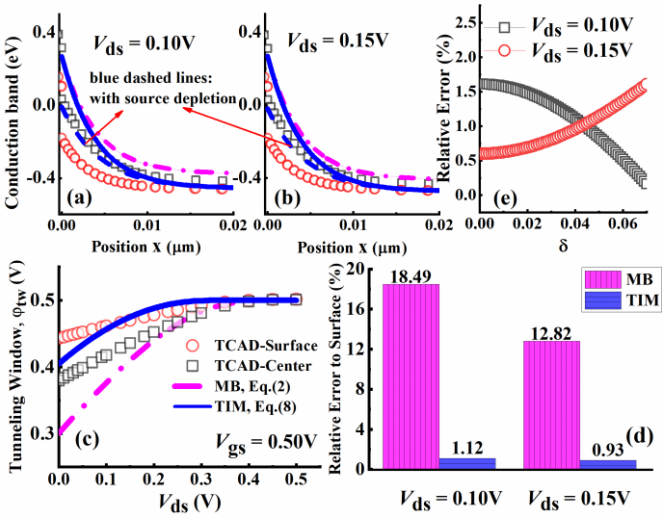

Fig. 3. CB profiles at (a) V_{ds} = 0.10V and (b) V_{ds} = 0.15V. (c) Curve of φ_{tw} vs. V_{ds}. (d) Histogram summarizing φ_{tw} relative error to surface value. (e) Relative error vs. δ. V_{gs} = 0.50V, d_2 = 0.2eV, and the other parameters are the same as in Fig. 1. The dashed lines in (a) and (b) show the case with source depletion.

$$F = F(V_{cv}) + F'(V_{cv})\left(V_{gs} - V_{cv}\right) + 0.5F''(V_{cv})\left(V_{gs} - V_{cv}\right)^2. \quad (7)$$

Then, the closed-form of φ_{tw} is written as

$$\varphi_{tw} = \varphi_{tw,TIM} = V_{gs} - \frac{F}{2C_{ox}}, \quad (8)$$

$$F = F_b\left[1 + \frac{C_{ox}}{V_t C_{ox} + 0.5F_b}\left(V_{gs} - V_{cv}\right) + \frac{0.5V_t C_{ox}^3}{\left(V_t C_{ox} + 0.5F_b\right)^3}\left(V_{gs} - V_{cv}\right)^2\right], \quad (9)$$

with $F_b = qt_sN_De^{(d_c-d_2)/V_t}$. Note that (8) cannot predict the potential in the saturation regime, i.e. the gate-control region. This is because after V_{cv} reaches V_{gs}, $\varphi_{tw,TIM}$ decreases with the continuing increase of V_{ds}. If all terms of V_{cv} in (9) are replaced by V_{gs}, a linear relationship between $\varphi_{tw,TIM}$ and V_{gs} (feature of gate-control region) is found. Finally, (8) can be used over the entire range, by exploiting the following contiguous function [13]

$$V_R = \frac{1}{2}\left[V_{gs} + V_{cv} - \sqrt{\left(V_{gs} - V_{cv}\right)^2 + \delta^2}\right], \quad (10)$$

to replace V_{cv} in (9). In (10), δ is a fitting factor for a smooth transition from gate-control to drain-control regions. In this paper, δ is set to 0.04V.

The analytical CB profiles obtained with (2) and (8) at V_{ds} = 0.10V and 0.15V, respectively, are presented in Fig. 3(a)-(b). The results of the corresponding numerical simulations are also plotted. Notice that the CB profile obtained with (8) is more accurate when comparing with the numerical results. As a consequence, a better match of the φ_{tw} vs. V_{ds} dependence is observed in Fig. 3(c) when using results from (8). Although, the saturation of φ_{tw} in the channel can be predicted by both TIM and MB, they deviate at lower V_{ds} from the TCAD result. This difference might come from the reduction of the three-dimensional to a one-dimensional problem. Despite this

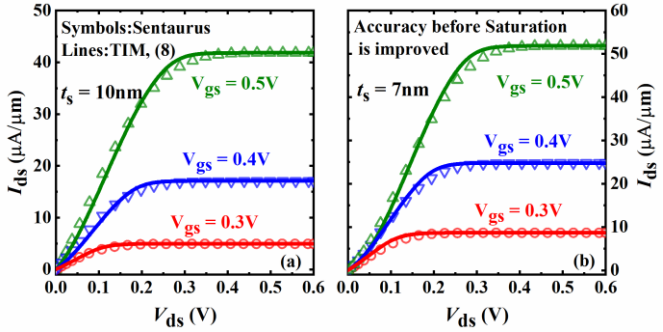

Fig. 4. I_{ds}–V_{ds} curves at various V_{gs} computed by means of TIM for H-TFETs with body thickness (a) t_s = 10 nm and (b) t_s = 7 nm. The simulation data in (a) are the same as in Fig. (1).

relatively crude approximation, the tunneling window obtained with TIM model is within the center and surface potential. The relative error of φ_{tw} w.r.t the simulated surface window, as shown in Fig. 3(d), reduces from 18.49% (12.82%) to 1.12% (0.93%), when it is modeled by TIM at V_{ds} = 0.10V(0.15V). Note that δ has a very small influence on the relative error (Fig. 3(e)). Therefore, the $I_{ds} - V_{ds}$ results from TIM are in better agreement with the numerical simulations, as shown in Fig. 4.

It may be confusing how the agreement is achieved when the CB barrier from model is bigger than that from simulation, as presented in Fig. 3. The same happens for the MB case. Actually, the two aspects, i.e. ignoring source depletion assumed in this paper and the consequent bigger CB barrier, lead to opposite effects on the current, counteracting each other's influence. The source depletion effects can be considered through the depletion approximation as in Refs. [14], [15], where $\varphi(x) = (E_{g,eff} - \Delta + q\varphi_{tw})\exp(-\pi x/\lambda) - q\varphi_{tw}$. Δ, being the energy bending of source depletion region, is the changed channel potential energy at x = 0 to keep the source band-gap constant, and can be obtained by the continuity conditions at the source/channel junction [14], [15]. As shown by the dashed lines in Fig. 3(a) and (b), a better match is obtained for the CB. Finally, in order to investigate the source doping influence, it might be necessary to include the hole tunneling contribution in (4) based on the source depletion potential (Fig. 2(a)). However, the latter would require the implementation of additional models [14] which are out of the scope of this work.

III. Conclusion

Based on TIM, an efficient and simple potential model is derived for H-TFET and verified by comparing with numerical simulations. The proposed method is fully analytical with no iterative steps involving the solution of a transport equation. It was found that TIM is more accurate than MB approximation to compute the tunneling window, leading to more accurate prediction for the $\boldsymbol{I_{ds} - V_{ds}}$ characteristics at a much less computational cost. Although, not discussed in detail here, the TIM model could accurately predict the $\boldsymbol{I_{ds} - V_{gs}}$ characteristic, especially at high gate voltages. Finally, trap-assisted tunneling which is likely to occur due to the technological immaturity of the chosen material system will not influence the result since it plays a major role in the subthreshold region [16], [17].

REFERENCES

[1] B. Rajamohanan, D. Mohata, A. Ali, and S. Datta, "Insight into the output characteristics of III–V tunneling field effect transistors," *Appl. Phys. Lett.*, vol. 102, no. 9, p. 092105, Mar. 2013, doi: 10.1063/1.4794536.

[2] L. Zhang and M. Chan, "SPICE modeling of double-gate tunnel-FETs including channel transports," *IEEE Trans. Electron Devices*, vol. 61, no. 2, pp. 300–307, Feb. 2014, doi: 10.1109/TED.2013.2295237.

[3] Y. Taur, J. Wu, and J. Min, "An analytic model for heterojunction tunnel FETs with exponential barrier," *IEEE Trans. Electron Devices*, vol. 62, no. 5, pp. 1399–1404, May 2015, doi: 10.1109/TED.2015.2407695.

[4] Y. Taur, J. Wu, and J. Min, "Dimensionality dependence of TFET performance down to 0.1 V supply voltage," *IEEE Trans. Electron Devices*, vol. 63, no. 2, pp. 877–880, Feb. 2016, doi: 10.1109/TED.2015.2508282.

[5] Y. Guan, Z. Li, W. Zhang, Y. Zhang and F. Liang, "An Analytical Model of Gate-All-Around Heterojunction Tunneling FET," *IEEE Trans. Electron Devices*, vol. 65, no. 2, pp. 776-782, Feb. 2018. doi: 10.1109/TED.2017.2783911.

[6] D. Li, B. Zhang, H. Lou, L. Zhang, X. Lin and M. Chan, "Comparative Analysis of Carrier Statistics on MOSFET and Tunneling FET Characteristics," *IEEE J. Electron Devices Soc.*, vol. 3, no. 6, pp. 447-451, Nov. 2015, doi: 10.1109/JEDS.2015.2475163.

[7] Q. Smets, A. S. Verhulst, S. El Kazzi, D. Gundlach, C. A. Richter, A. Mocuta, N. Collaert, A. V.-Y. Thean, and M. M. Heyns, "Calibration of the effective tunneling bandgap in GaAsSb/InGaAs for improved TFET performance prediction," *IEEE Trans. Electron Devices*, vol. 63, no. 11, pp. 4248–4254, Nov. 2016, doi: 10.1109/TED.2016.2604860.

[8] R. Pandey, N. Agrawal, V. Chobpattana, K. Henry, M. Kuhn, H. Liu, M. Labella, C. Eichfeld, K. Wang, J. Maier, S. Stemmer, S. Mahapatra, and S. Datta, "Tunnel junction abruptness, source random dopant fluctuation and PBTI induced variability analysis of $GaAs_{0.4}Sb_{0.6}/In_{0.65}Ga_{0.35}As$ heterojunction tunnel FETs," in *Proc. IEEE Int. Electron Devices Meeting (IEDM)*, Dec. 2015, pp. 14.2.1–14.2.4.

[9] K. M. Choi and W. Y. Choi, "Work-Function Variation Effects of Tunneling Field-Effect Transistors (TFETs)," *IEEE Electron Device Lett.*, vol. 34, no. 8, pp. 942-944, Aug. 2013, doi: 10.1109/LED.2013.2264824.

[10] *TCAD Sentaurus Manual*, Synopsys, Inc., Mountain View, CA, USA, 2013.

[11] E. O. Kane, "Theory of tunneling," *J. Appl. Phys.*, vol. 32, no. 1, pp. 83–91, Jan. 1961, doi: 10.1063/1.1735965.

[12] B. Lu, H. Lu, Y. Zhang, Yi M. Zhang, X. Cui, Z. Lv, S. Yang, and C. Liu, "A Charge-Based Capacitance Model for Double-Gate Tunnel FETs With Closed-Form Solution," *IEEE Trans. Electron Devices*, vol. 65, no. 1, pp. 299-307, Jan. 2018, doi: 10.1109/TED.2017.2775341.

[13] C. Wu, R. Huang, Q. Huang, C. Wang, J. Wang and Y. Wang, "An Analytical Surface Potential Model Accounting for the Dual-Modulation Effects in Tunnel FETs," *IEEE Trans. Electron Devices*, vol. 61, no. 8, pp. 2690-2696, Aug. 2014, doi: 10.1109/TED.2014.2329372.

[14] J. Min, J. Wu, and Y. Taur, "Analysis of source doping effect in tunnel FETs with staggered bandgap," *IEEE Electron Device Lett.*, vol. 36, no. 10, pp. 1094–1096, Oct. 2015, doi: 10.1109/LED.2015.2466676.

[15] Y. Dong, L. Zhang, X. Li, X. Lin, and M. Chan, "A Compact Model for Double-Gate Heterojunction Tunnel FETs," *IEEE Trans. Electron Devices*, vol. 63, no. 11, pp. 4506-4513, Nov. 2016, doi: 10.1109/TED.2016.2604001.

[16] S. Mookerjea, D. Mohata, T. Mayer, V. Narayanan, and S. Datta, "Temperature-dependent I–V characteristics of a vertical In0.53Ga0.47As tunnel FET," *IEEE Electron Device Lett.*, vol. 31, no. 6, pp. 564–566, Jun. 2010, doi: 10.1109/LED.2010.2045631.

[17] R. N. Sajjad, W. Chern, J. L. Hoyt, and D. A. Antoniadis, "Trap assisted tunneling and its effect on subthreshold swing of tunnel FETs," *IEEE Trans. Electron Devices*, vol. 63, no. 11, pp. 4380–4387, Nov. 2016, doi: 10.1109/TED.2016.2603468.